Peer review status:
This is a revised version of a preprint originally submitted to JGR: Solid Earth. The manuscript has now undergone peer review and has been updated accordingly.

Title:
The 'trench pull' force: constraints from elasto-plastic bending models

Author:
Dan Sandiford

Email:
dsand@unimelb.edu.au [Dan Sandiford]

The 'trench pull' force: constraints from elasto-plastic bending models

Dan Sandiford[1]

[1]University of Melbourne

Key Points:

- Trench pull refers to the net force associated with the pressure deficit beneath the trench, relative to an isostatic column in the trailing plate
- The force can be quantified by extending the concept of 'GPE*' to account for a corrected-density (ρ^*)
- Elasto-plastic plate models are used to constrain $\rho^*(z)$, suggesting a typical trench pull force of $\sim 2.5\ \mathrm{TN\,m^{-1}}$

Corresponding author: Dan Sandiford, dsand@unimelb.edu.au

Abstract

Stresses transmitted through slabs are thought to provide an important component of the driving force on the trailing plates. This 'net slab pull' is usually conceptualised in terms of in-plane differential stress, acting in the sense of tension. However, an additional component of the net slab pull arises from the vertical loading of the trailing plate, which is mediated through a pressure deficit created by plate downbending. The purpose of this paper is to investigate the mechanics and typical magnitude of this mechanism, which is termed the 'trench pull force'. The challenge is that because trench topography is non-isostatic, the relative pressure reduction depends on the vertical distribution of *horizontal gradients of the vertical shear stress*, e.g., $\frac{\partial \tau_{zx}}{\partial x}(z) \equiv \tau_{zx,x}(z)$. In the first part of the paper the concept of a gravitational potential energy difference and its relation to net horizontal forces is extended to include non-isostatic columns. This is achieved by introducing a corrected density distribution ($\rho^*(z)$), which incorporates effects of $\tau_{zx,x}$ via a pseudo-density ($\hat{\rho} = \frac{\tau_{zx,x}}{g}$). This gives rise to the corrected ΔGPE*, equal to the dipole moment of the difference in corrected density ($\Delta\rho^*(z)$). For a given trench deflection (w_T), the vertical center of mass of $\tau_{zx,x}(z)$ emerges as the key controlling parameter for the magnitude of the trench pull force. In the second part of the paper simple mechanical models are developed to explore the vertical distribution of $\tau_{zx,x}$ in a bending plate under load. These models highlight the tendency for $\tau_{zx,x}$ to concentrate at the center of the plate. Applying these models to the lithosphere implies that the trench pressure deficit acts over a length scale of $\frac{1}{2}z'_m$ where z'_m is the mechanical thickness. Based on this model a typical trench pull force is estimated to be about 2.5 $\mathrm{TN\,m^{-1}}$. The total topography that exists between ridges and trenches may be associated with a net driving force of about $5\mathrm{TN\,m^{-1}}$, enough to balance basal drag of 1 MPa over a plate length of 5000 km.

Plain Language Summary

The slab pull force derives from the excess buoyancy of plates that have been 'subducted' back into the mantle. Some fraction of this buoyancy force, mediated by the drag force that acts on the slab, seems capable of producing a horizontal driving force on the trailing plates. This is referred to as the 'net slab pull'. A common view is that slabs support stresses that act in the sense of a tension, which is transmitted all the way through the slab hinge to the trailing plate. However there is another mechanism, much less discussed, via which a net slab pull may be generated. Slab buoyancy pulls downward on the trailing plate, causing it to deflect several kilometers, and forming the long narrow depressions known as trenches. In the shallow subsurface beneath the trench axis a pressure deficit is anticipated compared with the same level in an non-deflected ('isostatic') point in the trailing plate. The pressure deficit creates the 'trench pull force', similar to the mechanism that 'pushes' from the younger shallower lithosphere to the older subsided parts (ridge push). While the magnitude of pressure deficit is easy to calculate, the primary uncertainly lies in understanding the vertical depth over which this pressure deficit persists. The models and assumptions developed in this study suggest that the trench pull force has a similar magnitude to the ridge push force: $\sim$ 2.5 $\mathrm{TN\,m^{-1}}$.

1 Introduction

Stresses propagated through slabs are thought to exert a important horizontal driving force on the trailing plate, know as the net slab pull. The prevailing conceptual model for net slab pull emphasizes the role of deviatoric in-plane stresses, as summarised by Davies (2022):

> Elsasser ... introduced the idea of the lithosphere as a stress guide, meaning that the tensional force from a sinking slab of lithosphere would propagate back into and along the attached surface plate, pulling it along after the sinking slab.

On spatial scales relevant to lithospheric dynamics, all principal stresses are compressional and the use of tension can be misleading (Richter et al., 1977). In the context of the above quote, tension simply refers to a state where the integrated down-dip normal stress is less compressional than the slab-perpendicular stress. For the trailing plate, this can be expressed in terms of vertical and horizontal stress difference. The vertical integral (or resultant) of this stress difference is symbolised F_D (as outlined in Section 2). In referring to this conceptual model for net slab pull, the term 'tensional' will be used.

A number of studies have discussed an alternative mechanism through which a net slab pull can develop (Richter et al., 1977; Bird, 1998; Bird et al., 2008; Bercovici et al., 2015) (there are likely be others the author is unaware of). As Richter et al. (1977) explain (symbols have been changed for consistency with this study):

> A driving force may arise in the same way as that at ridges. Because mantle rock is replaced by water, the lithostatic pressure at all depths is reduced by $(\rho_m - \rho_w)gw_T$, where w_T is the depth of the trench. However, unlike ridges, trenches are not isostatically compensated and must be maintained by elastic forces. Unfortunately, very little is yet known about the distribution of these stresses. It is not even clear whether any of the pressure reduction is available to drive the plates.

The term we adopt for this mechanism is the 'trench pull force', following Bird et al. (2008). The expression $(\rho_m - \rho_w)gw_T = \Delta P_T$ is referred to as the trench pressure deficit, which can be regarded as the source for the (potential) trench pull force. The down-bending of the trailing plate is often analysed using thin-plate flexure theory, in which the deflection is attributed to stress resultants acting across the vertical plane beneath the trench (Caldwell et al., 1976; Parsons & Molnar, 1976; Turcotte et al., 1978; Turcotte & Schubert, 2002; Garcia et al., 2019). These resultants arise from a state of differential stress.

Both mechanisms for generating net slab pull imply that the subduction hinge can maintain a state of differential stress over extended periods, functioning as a stress guide. They differ however, in respect to the stress distributions that would be anticipated on a vertical plane at the edge of the trailing plate. Specifically, the tensional mode would be associated with a positive in-plane resultant ($F_D(x_T) > 0$, using the symbol adopted in this current study), while the trench pull mode will be associated with a vertical shear stress resultant $V(x_T)$ and/or bending moment $M(x_T)$, where x_T represents the location of the trench. Section 2 provides the quantitative definitions for these terms, and a summary is given Table 1.

As noted by Richter et al. (1977), trench pull exhibits both similarities to and differences from ridge push — the more familiar topographic driving force on the trailing plate. Both forces will be seen to arise from an identical integral quantity, specifically: $\Delta\bar{\sigma}_{zz}$, where σ_{zz} is the vertical normal stress, the bar represents vertical integration to an assumed compensation level (z_c), and the Δ represents the difference in integrated values between the two columns (across which a net force is to be determined). The quantity $\Delta\bar{\sigma}_{zz}$ arises when we consider a particular form of a vertically integrated horizontal force balance. The derivation is given in Section 2, clarifying why vertical stress appear at all in a horizontal force balance.

$\Delta\bar{\sigma}_{zz}$ is a general expression which can be evaluated for any two columns of lithosphere. Fundamentally, what defines the trench pull force is the choice of columns:

$$\text{trench pull force} \equiv -\Delta\bar{\sigma}_{zz} \\ = -(\bar{\sigma}_{zz}(x_I) - \bar{\sigma}_{zz}(x_T)) \quad (1)$$

Where $x = x_T$ denotes the column beneath the trench, and $x = x_I$ denotes an isostatic column at the same age. The negative sign in Eq. 1 relates to the convention for the stress tensor and will be clarified in Section 2.

When lithospheric columns are isostatic, it is generally appropriate to substitute the lithostatic pressure $P_L(z)$ for $-\sigma_{zz}(z)$. In this case, $\Delta\bar{\sigma}_{zz} = \Delta\text{GPE}$, where GPE refers to the gravitational potential energy per unit area. When the distribution of vertical shear stress plays a role in supporting the topography, we cannot make this substitution as $P_L(z) \neq -\sigma_{zz}(z)$. Note that $\Delta\bar{\sigma}_{zz}$ still remains a completely valid expression of a (potential) net horizontal force between columns, but that force is no longer equal to the GPE difference.

The structure of the paper is as follows. Section 2 develops the mathematical framework, starting with the static equilibrium relation, and developing the vertically-integrated form of the horizontal force balance from which emerges the key term $\Delta\bar{\sigma}_{zz}$. Next, the framework for GPE differences is extended to include non-isostatic columns by treating *horizontal gradients in vertical shear stresses* as a pseudo-density. The development here is general, and not confined to the trench pull problem. In Section 3, simple mechanical models are introduced to explore how vertical shear stress gradients are distributed in the bending plate near the trench. Section 4 combines these results to provide an estimate of the typical trench pull force. Section 5 provides a brief discussion on some of the implications, observations and tests that are relevant to further investigation of the trench pull mechanism.

2 Model equations and assumptions

2.1 Preliminaries

To define a length scale over which the downbending occurs, we consider the distance L_T between trench (x_T) and the nearest isostatic column in the trailing plate (x_I, also called the first zero crossing). Previous investigations suggest $L_T \sim$ 50-100 km (Caldwell et al., 1976). The fact that $\lambda \ll R_e$, warrants the use of flat Earth (local Cartesian) approximation, rather a description based on rotations around the center or Earth (with radius R_e). Likewise, the along-strike extent of trenches being generally much greater than z'_m (the mechanical thickness of the lithosphere), warrants a 2D, plane strain approximation. Specifically, this asymmetry means we can neglect out-of plane flexural support of the trench topography. These approximations are standard in the analysis of and trench flexure and topographic force contributions (Parsons & Molnar, 1976; Caldwell et al., 1976; Molnar & Lyon-Caen, 1988; Lister, 1975).

The conservation of linear momentum in a continuum is expressed in Cauchy's momentum equation. In lithospheric dynamics the contribution of inertia is negligible and the conservation equations reduce to the static equilibrium condition:

$$\sigma_{ij,j} + \rho\delta_{iz}\, g = 0 \quad (2)$$

where σ_{ij} is the symmetric stress tensor, and the term $\rho g\delta_{iz}$ represents the body force per unit volume due to gravity, acting in the vertical direction. Applying Gauss' theorem we can write the local equilibrium relation in terms of a volume element:

$$\int_{\partial V} \sigma_{ij} n_j \, dA + \int_V \rho g \delta_{iz} \, dV = 0 \tag{3}$$

where n_j is the outward normal to the surface ∂V (the boundary of the volume V) and dA is the surface area element. We use the continuum-mechanics convention of stress being negative in compression.

Since horizontal forces must balance in static equilibrium, the integrated tractions in the x direction must vanish:

$$\int_{\partial V} \sigma_{xj} n_j \, dA = 0 \tag{4}$$

Fig. 1 shows an idealised section of a trailing plate extending from the trench to an arbitrary seaward location. As shown in the figure, two vertical coordinate systems will be referred to. The z system represents vertical distance from a fixed equipotential datum. Because we assume constant vertical gravity, equipotential surfaces are always surfaces of constant z. We will use $z_I = z_s(x_I)$ to represent the isostatic level of an idealised column of the lithosphere with the same age (density structure) as the lithosphere are the trench axis. We will also write: $z_s(x) = z_I + w(x)$, where $w(x)$ is a standard symbol for the non-isostatic deflection. The z' system denotes depths relative to the plate surface. This local system is more appropriate for describing quantities such as the mechanical thickness (z'_m), or the thermal thickness (z'_t).

2.2 The vertically-integrated horizontal force balance

We now apply the horizontal static equilibrium equation (Eq. 4) to a finite volume representing a section of lithosphere, as shown in Fig. 1. The symbol Ω_k is used to represent the ($k =$)4 non-overlapping boundaries. Traction integrations across these boundaries give rise to force components (per unit distance in the out plane direction). To keep the derivation as general as possible, we will refer to the location of Ω_0 as x_0 and the Ω_1 as x_1; later we will consider the specific case of this general force balance when x_0 is located at the trench (denoted x_T), and x_1 is the location of an isostatic column at the same age (x_I).

The choice of the rectangular domain allows for a key simplification: the only contribution to the horizontal traction components ($\sigma_{xj} n_j$) in Eq. 4 comes from the horizontal normal stress (σ_{xx}) in the case of the vertical boundaries, and the horizontal shear stress ($\sigma_{xz} = \tau_{xz}$), in the case of the top and bottom boundary. This means that only the sign of the dot product in Eq. 4 is relevant, and we can write:

$$\begin{aligned} &- \int_{\Omega_0} \sigma_{xx}(x_0, z) dz + \int_{\Omega_1} \sigma_{xx}(x_1, z) dz \\ &+ \int_{\Omega_2} \tau_{xz}(x, z_c) dx - \int_{\Omega_3} \tau_{xz}(x, z_0) dx = 0 \end{aligned} \tag{5}$$

The top boundary (Ω_3) represents the water-air interface; tractions associated with the shear stress are negligible and the final term in Eq. 5 can be neglected. The inclusion of the water column in the force balance warrants explanation. An alternative choice would be to define the domain such that the top boundary is the rock-water interface. In this case, it is still warranted to neglect shear stresses, however the hydrostatic pressure acting on the outer slope is relevant. Assuming an isostatic level appropriate for old lithosphere (e.g, 4 km) with an additional deflection of + 3.5 km at the trench axis, the resulting net force due to pressure acting on the vertical projection of the outer slope is ≈ 0.2 TN m^{-1}. When we consider the combined (rock + water) domain shown in Fig.

1, this contribution gets subsumed as a change in the net force component described by $\Delta\bar{\sigma}_{zz}$. This study concludes that the change is minor relative to the typical magnitude of the trench pull force.

The integration depth in Eq. 5 (z_c) represents a distance relative to the fixed system (z), and hence an equipotential surface. In general, the principle of a compensation depth/level is motivated by the inference that most of the long-wavelength topography signal on Earth is isostatically compensated (Watts, 2001; Turcotte & Schubert, 2002). In this study we adopt the standard hydrostatic assumption, which implies that trench deflection is completely supported due to the presence of a vertical shear stress within the lithosphere, rather than a being a manifestation of pressure gradients in the asthenosphere (Caldwell et al., 1976; Turcotte & Schubert, 2002; Garcia et al., 2019).

We now choose a more compact notation, introducing the overbar symbol to represent the vertical integral from z_0 to z_c, and the Δ symbol to represent the difference between columns. Eq. 5 can be then written:

$$\Delta\bar{\sigma}_{xx} + \int_{\Omega_2} \tau_{xz}(x, z_c)dx = 0 \tag{6}$$

$$\text{with } \Delta\bar{\sigma}_{xx} = \bar{\sigma}_{xx}(x_1) - \bar{\sigma}_{xx}(x_0)$$
$$\text{and } \bar{\sigma}_{xx}(x) = \int_{z_0}^{z_c} \sigma_{xx}(x, z)dz$$

Eq. 6 states that the difference in integrated horizontal normal stress, must balance the integrated shear stresses on the base. It is also commonly expressed in a differential form (Fleitout & Froidevaux, 1983). A positive change either of the quantities in Eq. 6 from $x_0 \to x_1$ represents a force to the right. Although Eq. 6 might be regarded as the fundamental statement of the horizontal force balance, it has limited value in terms of understanding different contributions to the lithospheric force balance. We consider an alternative representation, first by expanding the normal stress (σ_{xx}) into the deviatoric/isotropic components ($\tau_{xx} + \sigma_{\mathrm{I}}$), and then expanding the mean stress in terms of vertical stress quantities: $\sigma_{\mathrm{I}} = \sigma_{zz} - \tau_{zz}$. Making these substitutions in the LHS of Eq. 6 gives:

$$\Delta(\overline{\tau_{xx} - \tau_{zz}}) + \Delta\bar{\sigma}_{zz} + \int_{\Omega_2} \tau_{xz}(x)dx = 0 \tag{7}$$

The first term on LHS of Eq. 7 represents the difference between columns (Δ) of the resultant of the quantity $(\tau_{xx}(z) - \tau_{zz}(z))$. We refer to $(\overline{\tau_{xx} - \tau_{zz}})$ as the in-plane differential stress resultant, symbolized F_D. The second term in Eq. 7 reflects the way vertical normal stress distribution impacts the integrated mean stress. In this study, we use the symbol GPE* to represent the negative of quantity $\bar{\sigma}_{zz}$. The final term in Eq. 7 is the basal shear force, which will be represented by F_B. Over the length-scale of the trench topography (L_T) F_B is likely to be negligible. The Δ symbols mean that without knowing boundary conditions, solutions to Eq. 7 can be only determined up to an additive constant. In symbolic form we will write:

$$\Delta F_D - \Delta\mathrm{GPE}^* + F_B = 0 \tag{8}$$

Note the deliberate use of the asterisk on the second term, which is intended to read as the 'corrected-GPE'. The fundamental definition of GPE* is the (negative of) the vertical integral of 'true' vertical normal stress $\bar{\sigma}_{zz}$. In general, GPE* $\neq$ GPE. The quantities are only equal when the vertical normal stress in both columns is lithostatic. This point is elaborated in following sections. The sign definition (GPE$^* = -\bar{\sigma}_{zz}$) is to align GPE* with the standard convention, the *true* GPE being defined in terms of a positive lithostatic pressure. This now also means that a positive change in the GPE* from $x_0 \rightarrow x_1$ represents a force to the left. This is in contrast to first and last terms in Eq. 8, which retain the same directional sense as Eq. 7. We now note the equivalent definitions:

$$\begin{aligned} \text{trench pull force} &\equiv -(\bar{\sigma}_{zz}(x_I) - \bar{\sigma}_{zz}(x_T)) \\ &= \text{GPE}^*(x_I) - \text{GPE}^*(x_T) \\ &= \Delta\text{GPE}^* \end{aligned} \tag{9}$$

2.3 The vertical force balance

In order to estimate the trench pull force, we need to develop a model for the distribution of vertical normal stress in each column. Expanding Eq. 2 for the z component, yields:

$$\frac{\partial \sigma_{zz}}{\partial z} + \frac{\partial \tau_{zx}}{\partial x} + \rho g = 0 \tag{10}$$

Integration of Eq. 10 from the vertical origin (z_0) to an arbitrary depth (z) yields the distribution of the vertical normal stress, where ζ is a dummy variable:

$$\sigma_{zz}(x,z) = -\int_{z0}^{z} \rho(x,\zeta) g d\zeta - \int_{z0}^{z} \frac{\partial \tau_{zx}}{\partial x}(x,\zeta) d\zeta \tag{11}$$

The first term on the RHS of Eq. 11 is called the lithostatic pressure ($P_L(x,z)$). The second term on the RHS represents the way in which gradients of the vertical shear stress impact the vertical force balance. Schmalholz et al. (2014) refer to the this as the shear function, symbolized $Q(z)$. Comma notation is used for partial derivatives to keep the mathematical expressions concise: $\frac{\partial \tau_{zx}}{\partial x} \equiv \tau_{zx,x}$.

2.4 Flexural Isostasy

The hydrostatic assumption requires that the LHS of Eq. 11 is invariant at the compensation level z_c. When $\tau_{zx,x}(z)$ has a finite resultant (i.e. $\bar{\tau}_{zx,x} \neq 0$), the lithosphere must deflect vertically ($w(x)$) from its isostatic level, leaving the LHS unperturbed. For a given deflection from the isostatic level the change in the lithostatic term (the weight of the column above z_c) is: $-(\rho_m - \rho_w) g w(x)$. This expresses the fact that vertical motion of a column results in the substitution of material at the compensation level with the material that lies above the rock surface, in this case mantle rock with seawater. The sign is due to the fact that for a positive w there is a loss of weight in the column. Therefore for any column:

$$\int_{z_0}^{z_c} \frac{\partial \tau_{zx}}{\partial x}(x,z) dz = \int_{z_0}^{z_c} -\Delta\rho(x,z) g dz \tag{12}$$

$$\text{or,} \quad \bar{\tau}_{zx,x}(x) \approx -(\rho_m - \rho_w) g w(x) \tag{13}$$

where the $\Delta\rho(z)$ represents the difference in density between the isostatic reference column and the density in the same column when deflected by a distance w. The approximate sign reflects that fact we will ignore the contributions to $\Delta\rho(z)$, that arise form a vertical offset of the crustal and thermal density structure. This assumption is discussed in Appendix B. If we exchange the order of integration and differentiation in Eq. 13, the connection with the vertical force balance as expressed in the thin plate flexure model becomes clear. In thin plate flexure, the integral of the vertical shear stress across the plate is termed the vertical shear stress resultant, and is usually symbolised V (Turcotte & Schubert, 2002):

$$\begin{aligned}\frac{\partial}{\partial x}\int_{z_0}^{z_c}\tau_{zx}(x)dz &= -(\rho_m-\rho_w)gw(x)\\ \frac{\partial}{\partial x}V(x) &= -(\rho_m-\rho_w)gw(x)\end{aligned} \tag{14}$$

2.5 A corrected GPE* for non-isostatic columns

We can interpret $\tau_{zx,x}$ as a pseudo-density, by writing, $\hat{\rho}(z)=\frac{\tau_{zx,x}(z)}{g}$. Allowing Eq. 13 to be written:

$$\int_{z_0}^{z_c}\hat{\rho}(x,z)dz = -(\rho_m-\rho_w)w(x) \tag{15}$$

and define a corrected-density, $\rho^*(z)=\rho(z)+\hat{\rho}(z)$, such that for any two columns:

$$\int_{z_0}^{z_c}\Delta\rho^*(z)dz = \int_{z_0}^{z_c}\left(\Delta\rho(z)+\Delta\hat{\rho}(z)\right)dz = 0 \tag{16}$$

This is the flexural-isostatic statement that all columns reach the same vertical normal stress at the compensation level, or equivalently that the pseudo-mass anomaly in a column balances the true mass anomaly due to the deflection. Following this approach, we can define a corrected GPE*:

$$\begin{aligned}\mathrm{GPE}^*(x) &\equiv -\bar{\sigma}_{zz}(x)\\ &= -\int_{z_0}^{z_c}\sigma_{zz}(x,z)dz\\ &= \int_{z_0}^{z_c}\left(P_L^*\right)dz\\ &= g\int_{z_0}^{z_c}\left(\int_{z_0}^{z}\rho^*(x,\zeta)d\zeta\right)dz\end{aligned} \tag{17}$$

where $P_L^*(z)$ refers to a corrected lithostatic pressure, i.e., the overburden weight in a column where the true density has been corrected to account for the effects of $\tau_{zx,x}(z)$. Eq. 17 can be transformed into a single integral by reversing the order of integration:

$$\mathrm{GPE}^*(x) = g\int_{z_0}^{z_c}\rho^*(x,z)(z_c-z)dz \tag{18}$$

where the (corrected) density distribution is weighted by the height above the integration depth (z_c-z). The *difference* in GPE* between two columns can be written:

$$\Delta\mathrm{GPE}^* = g\int_{z_0}^{z_c}\Delta\rho^*(z)(z_c-z)dz \tag{19}$$

Eq. 19 represents the dipole moment of the difference in corrected density distribution $\Delta\rho^*(z)$. This is a generalisation of the expression for isostatic columns, written in terms of $\Delta\rho(z)$ (Turcotte & Schubert, 2002). The magnitude of the dipole moment depends on the product of a force and a moment arm. Under assumptions applicable to the trench pull force, it can be shown (Appendix B) that the moment-arm distance is completely specified by the vertical center of mass of $\tau_{zx,x}(z)$ in the non-isostatic column, and therefore that the ΔGPE^* is completely controlled by the depth distribution of $\tau_{zx,x}(z)$. The challenge will be understanding this distribution; this is the topic of Section 3. It should also be noted that the three 'corrected' quantities we have introduced: density ρ^*, lithostatic pressure $P_L^*(z)$, and GPE* are mathematical constructs. These only have relevance in terms of how vertically integrated quantities affect the horizontal force balance. In other words, the pseudo-density ($\hat{\rho}(z)$) has no relevance in terms of the gravitational effects arising from a column, which depend only on the true density $\rho(z)$.

2.6 Parameters and reference values

A primary objective of this paper is to develop an estimate for the magnitude of the trench pull force, i.e., the $-\Delta\bar{\sigma}_{zz} \equiv \Delta\text{GPE}^*$ between a column at the trench compared with an isostatic reference column of the same age. In discussing a typical value for trench pull, our attention will focus on capturing the behavior of older lithosphere ($>$ 80 Myr). This is similar to the way in which the ridge push force is usually quoted in the range of 2-4 $\text{TN}\,\text{m}^{-1}$, which is an estimate applicable to the subsidence of old lithosphere (Lister, 1975; Turcotte & Schubert, 2002; Coblentz et al., 2015). Global studies of trench bathymetry suggest that relative trench depths for older lithosphere lie in the range of about 2.5 - 5.5 km and exhibit a positive correlation with the age of the subducting plate at the trench (Grellet & Dubois, 1982). A value of 3.5 km is chosen as representative for old lithosphere, but clearly there are significant variations around this value (Grellet & Dubois, 1982; Zhang et al., 2014; Lemenkova, 2019). Table 1 shows additional reference values for parameters such as z'_m, the mechanical thickness of the lithosphere. These values are introduced and explained throughout the remainder of the study.

3 The distribution of vertical shear stress in bending plates

In this section we discuss solutions for the depth distribution of the vertical shear stress ($\tau_{zx}(z)$) and its horizontal gradients $\tau_{zx,x}(z)$, for the flexure of uniform elastic, and elasto-perfectly plastic plates.

3.1 Elastic plates

In the thin-plate flexure model, vertical shear stresses only appear in terms of the resultant quantity (V), e.g., Eq. 14 and the depth distribution is ignored. Analytic solutions that describe the shear stress distribution can be derived through Airy's method (or stress functions). These are detailed in continuum mechanics references, where simple loading loading examples are discussed (Goodier & Timoshenko, 1970). We can approach the solution more directly however, with only the usual assumptions for thin plate flexure (plane bending, zero shear stress on the top and bottom edge) and the stress equilibrium relation (Eq. 2). In this section the vertical coordinate (z) has its origin at the center of the plate, the orientations remain positive down and to the right. As derived in Appendix A, the distribution of vertical shear stress for an elastic plate of thickness h is parabolic:

$$\tau_{zx}(x,z) = \frac{V(x)}{I}\left(\frac{z^2}{2} - \frac{h^2}{8}\right) \tag{20}$$

Symbol	Explanation	Related equation	reference value [unit]
x_I	x loc. of isostatic column	-	- [km]
x_T	x loc. of trench	-	- [km]
L_T	trench length scale	$x_I - x_T$	100 [km]
$z_S(x)$	surface of plate	-	- [km]
$w(x)$	deflection relative to $z(x_I)$	$z_S(x) - z_S(x_I)$	- [km]
w_T	deflection at trench	$z_S(x_T) - z_S(x_I)$	3.5 [km]
z_I	z loc. of isostatic column	$z_S(x_I)$	- [km]
z_T	z loc. of trench axis	$z_S(x_T) = z_I + w_T$	- [km]
z_c	depth of vertical integration	$z_I + z'_t$	$\approx$ 100 [km]
z'_m	mechanical thickness	-	60 [km]
z'_{np}	neutral plane depth	$\approx \frac{1}{2} z'_m$	30 [km]
z'_t	thermal thickness	-	100 [km]
ΔP_T	trench pressure deficit	$(\rho_m - \rho_w) g w_T$	$\approx$ 80 [MPa]
F_{D}	in-plane resultant	$(\overline{\tau_{xx} - \tau_{zz}})$	- [$\mathrm{TN\,m^{-1}}$]
V	vertical shear stress resultant	$\bar{\tau}_{zx}$	- [$\mathrm{TN\,m^{-1}}$]
$\tau_{zx,x}$	vertical shear stress gradient	$\equiv \frac{\partial \tau_{xz}}{\partial x}$	- [$\mathrm{N\,m^{-3}}$]
ρ	density	-	- [$\mathrm{kg\,m^{-3}}$]
$\hat{\rho}$	pseudo-density	$\frac{\tau_{zx,x}}{g}$	- [$\mathrm{kg\,m^{-3}}$]
ρ^*	corrected density	$\rho + \hat{\rho}$	- [$\mathrm{kg\,m^{-3}}$]
$P_L(z)$	lithostatic pressure	$\int_{z0}^{z} \rho(x,\zeta) g d\zeta$	- [MPa]
$P_L^*(z)$	corrected lithostatic pressure	$\int_{z0}^{z} \rho^*(x,\zeta) g d\zeta$	- [MPa]
GPE	true GPE	$\bar{P}_L$	- [$\mathrm{J\,m^{-2}}$]
GPE*	corrected GPE	$\bar{P}_L^* = -\bar{\sigma}_{zz}$	- [$\mathrm{J\,m^{-2}}$]
g	gravity	-	9.8 [$\mathrm{m/s^2}$]
ρ_m	mantle density	-	3300 [$\mathrm{kg\,m^{-3}}$]
ρ_w	water density	-	1000 [$\mathrm{kg\,m^{-3}}$]
Δ	difference between columns	-	-

Table 1. Symbols, definitions, reference parameters and standard units used discussed in this paper. Overbars represent vertical integration across the lithosphere, from $z_0 \rightarrow z_c$

where I is the (2D) second moment of the area per unit length. Note that in Eq. 20, V represents the shear stress resultant, meaning the expression on the RHS (excluding V) defines a unit parabola:

$$\hat{\varphi}(z) = \frac{1}{I}\left(\frac{z^2}{2} - \frac{h^2}{8}\right) \tag{21}$$

$$\int_{-\frac{h}{2}}^{\frac{h}{2}} \hat{\varphi}(z)\, dz = 1 \tag{22}$$

Because $\hat{\varphi}$ is independent of x, the horizontal gradient is also parabolic (e.g., Tanimoto (1957)):

$$\tau_{zx,x}(z) = \hat{\varphi}(z)\frac{dV(x)}{dx} \tag{23}$$
$$= -\hat{\varphi}(z)f(x) \tag{24}$$

where we have used $\frac{dV(x)}{dx} = -f$, i.e., the expression of vertical force balance in terms of the shear stress resultant (see Eq. 14, or Appendix A). Eq. 24 states that for a uniform 2D elastic plate under the given boundary conditions, the vertical shear stress is always parabolic, and that along the plate, the parabola stretches with a gradient that is proportional to the load (f). When thin-plate models are applied to subduction zones, the loading pattern typically consists of a combination of end loads (e.g, $V(x_T)$), end moments (e.g, $M(x_T)$), while the normal load is due to the hydrostatic restoring force (Turcotte & Schubert, 2002). However, to visualise the stress distributions in plane bending, a simpler loading pattern is sufficient.

Fig. 2 shows a diagram of the deflection of an elastic plate by a uniformly distributed normal force. The right hand boundary is free, the left boundary is clamped. The deflection, as well as the maximum horizontal stress (σ_{xx}^{Max}) and shear stress (τ_{zx}^{Max}) have analytic solutions, as described in the figure caption. Fig. 3 shows stress components along the profile locations shown in Fig. 2. The upper panels of Fig. 3 show the stress distribution at 2 points in the elastic domain (e1, e2). These profiles emphasise the relationships developed in this section. Of particular importance is the parabolic distribution of $\tau_{zx,x}(z)$. This implies an identical shape for the pseudo-density $\hat{\rho}(z)$, which reaches its maximum at (and is symmetric around) the plate center.

3.2 Extension to elastic-plastic plates

In the trench region, the trailing plate is expected to undergo comprehensive yielding and approaches moment saturation. This behavior is predicted from yield stress envelopes (YSEs) (Chapple & Forsyth, 1979; McNutt & Menard, 1982), and is exhibited in numerical models which incorporate analogous constitutive models (Bessat et al., 2020; Sandiford & Craig, 2023). Yielding has an important impact on the depth distribution of vertical shear stress (and its gradients) as has been highlighted in engineering literature on bending plates (Horne, 1951; Drucker, 1956). Following Horne (1951) we adopt an elasto-perfectly-plastic model, where the maximum shear stress is truncated at a prescribed limit, giving rise to the plastic zones shown in grey in Fig. 2, and the truncated horizontal stress profiles shown on the lower left panel of Fig. 3.

To appreciate the impact on the vertical shear stress, consider the statement of horizontal stress equilibrium (Eq. 2) expanded in the horizontal coordinate:

$$\frac{\partial \sigma_{xx}}{\partial x} + \frac{\partial \tau_{xz}}{\partial z} = 0 \tag{25}$$

Yielding implies that first term, the horizontal gradient of the horizontal normal stress, is zero. It follows that the second term, the vertical gradient of the *horizontal* shear stress, is also zero:

$$\frac{\partial \sigma_{xx}}{\partial x} = 0 \implies \frac{\partial \tau_{xz}}{dz} = 0 \tag{26}$$

The boundary condition on the shear stress at either edge of the plate is assumed to be zero, and so the *horizontal* shear stress must be zero throughout the plastic regions; by symmetry so is the vertical shear stress (τ_{zx}). The same conclusions are developed in greater detail in Horne (1951). In the interior of the elastic core region, the vertical shear stress will remain parabolic, as long as the horizontal normal stress stress distribution remains linear in z (plane bending). In the yielding region, gradients in vertical shear shear stress ($\tau_{zx,x}(x,z)$) will now depend on the rate at which the elastic core is narrowing, as well as the normal force $f(x)$. Solutions to this type of problem require non-linear approaches (Turcotte et al., 1978).

Vertical profiles of the elasto-plastic stress state (p1, p2) are shown in the lower panels of Fig. 3. Following Horne (1951), $\tau_{zx}(z)$ takes the form of a truncated parabola. In the limit $\Delta x \rightarrow 0$, a piecewise analysis implies the same truncated parabola for $\tau_{zx,x}$ (lower right hand panel). In the limit of the elastic core becoming very thin, the magnitudes of the vertical shear stress and its gradient grow commensurately - potentially approaching the yield bounds Horne (1951). In terms of $\tau_{zx,x}(z)$, or equivalently $\hat{\rho}(z)$, this results in a vertical force balance contribution that increasingly resembles a point load concentrated at the midplane of the plate.

An important observation is that the center of mass of $\tau_{zx,x}(z)$ (or $\hat{\rho}(z)$) does not change with progressive yielding. Note that if an elasto-plastic plate begins to unbend, vertical shear stress gradients (finite $\tau_{zx,x}(z)$) may re-emerge in the depth region where previously they were constrained (by yielding) to be zero. This may be relevant, as models of plate bending often predict that the maximum bending moment occurs slightly seaward of the trench (Turcotte et al., 1978; Sandiford & Craig, 2023).

4 Estimating the trench pull force

4.1 Summary of the development so far

A form of vertically-integrated horizontal force balance has been developed (Eq. 7) which includes a force contribution given by $\Delta\bar{\sigma}_{zz}$. This term represents a 'generic' contribution which may be evaluated for any two columns. The trench pull force is defined by the evaluating $\Delta\bar{\sigma}_{zz}$ for two specific columns, x_T and x_I (e.g., Eq. 1). We defined a 'corrected' GPE* such that $\Delta\text{GPE}^* = -\Delta\bar{\sigma}_{zz}$. We showed that ΔGPE^* can be expressed as the dipole moment of the difference in the corrected density $\Delta\rho^*(z)$, between columns (Eq. 19). The corrected density includes the contribution of gradients in the vertical shear stress via a pseudo-density $\hat{\rho}(z) \propto \tau_{zx,x}$. This extends the classical framework which links the differences in (true) GPE to a net horizontal force, to include non-isostatic columns. GPE* is not a redefinition of true GPE, simply a mathematical construct to understand horizontal force components arising from $\Delta\bar{\sigma}_{zz}$. Application of the mechanical models and assumption from the previous section, provides insight in the depth distribution of $\tau_{zx,x}(z)$. Adopting these models for the distribution of $\hat{\rho}(z)$ in the column beneath the trench will allow us to define $\Delta\rho^*(z)$ and compute the ΔGPE^*. This approach enables both a general expression for the trench pull force, and a specific estimate based on the reference parameters from Table 1

4.2 Further assumptions

Determining a depth distribution for $\Delta\rho^*(z)$, rests on 3 main assumptions: first we make the assumption that the only non-negligible contribution to the true density difference ($\Delta\rho(z)$) arises from the contrast between rock and water. This means that $\Delta\rho(z)$ is finite only within the depth interval between the isostatic level ($z_s(x_I)$) and deflected level ($z_s(x_T)$). See Appendix B for further discussion. Secondly we assume that the pseudo-density is negligible in the isostatic column: $\hat{\rho}(x_I, z) \propto \tau_{zx,x}(x_I, z) = 0$. This implies that the $\Delta\hat{\rho}(z) = -\hat{\rho}(x_T, z) \propto \tau_{zx,x}(x_T, z)$. In other words, the distribution of $\Delta\hat{\rho}(z)$ is completely determined by the stress distribution chosen for the trench column, i.e. $\tau_{zx,x}(x_T, z)$.

This brings us to the final assumption which relates to applying the models developed in Section 3, which were based on plates with an unambiguous thickness (h). The assumption here is that in applying these models to the lithosphere we take $h \approx z'_m$. This equivalence arises because only the lithospheric layer above z'_m can sustain appreciable differential stress over geologically relevant timescales. In the application of the models from Section 3, we will therefore assume that the distribution of $\tau_{zx,x}(x_T, z)$ is finite within - and symmetric across - the depth interval $z_S(x_T)$ and $z_S(x_T) + z'_m$. In other words, across the mechanical thickness of the deflected column.

4.3 Expression for the trench pull force

The depth distribution of corrected density $\Delta\rho^*(z)$ is shown in the left panel of Fig. 4. Positive values represent the contribution of the true density contrast $\Delta\rho(z)$, negative values represent the contribution of the pseudo-density contrast $\Delta\hat{\rho}(z)$. Note that as per Eq. 16, the sum of the $\Delta\rho(z)$ and $\Delta\hat{\rho}(z)$ is zero - this may not be readily apparent as the length scales are different on the positive and negative sides.

The black lines in Fig. 4 show three possible distributions for $\tau_{zx,x}(x_T, z)$, which uniquely determine the $\Delta\rho^*(z)$, as per the discussion in the previous section. Two of these models are physically motivated, corresponding to the elastic and elasto-plastic distributions for $\tau_{zx,x}(z)$ (the latter for an arbitrary degree of yielding). The third distribution, $\tau_{zx,x}(z) = \text{constant}$, is shown with the solid black line. This model is not physically consistent, as it doesn't satisfy the boundary conditions or the equilibrium equations. However, because each of the distributions have the same integrated value, and same center of mass, the contribution to the GPE* is identical.

Fig. 4 illustrates two ways of interpreting the magnitude of the ΔGPE* (and hence the trench pull force). Firstly, the ΔGPE* corresponds to the area bounded by $\Delta\sigma_{zz}(z)$, as shown in the middle panel of Fig. 4. Each of the models shown in black lead to equal area. The model of constant $\tau_{zx,x}(z) = \text{constant}$ is useful as it leads to a ΔGPE* integral that can be calculated by inspection. This is represented in the combined area of the two grey triangles in the middle panel of Fig. 4. The magnitude of the trench pull force can therefore expressed:

$$
\begin{aligned}
-\Delta\bar{\sigma}_{zz} \equiv \Delta\text{GPE}^* &= (\rho_m - \rho_w) g w_T \left(\frac{w_T + z'_m}{2}\right) \\
&\approx \Delta P_T \left(\frac{z'_m}{2}\right) \\
&\approx \Delta P_T \left(z'_{np}\right)
\end{aligned}
\tag{27}
$$

For the reference parameters (Table 1), the estimated trench pull force is ≈ 2.5 TN m^{-1}. The use of $\approx$ in Eq. 27 discussed in the Fig. 4 caption.

From Eq. 19, the ΔGPE* is also equal to the dipole moment of $\Delta\rho^*(z)$ (see also Appendix B). The dipole length is shown schematically in the left hand panel Fig. 4. Because ΔP_T, as well as the center of mass of $\Delta\rho$ are fixed, the ΔGPE* is completely determined by the center of mass of the pseudo-density $\Delta\hat{\rho}(z)$, which is uniquely determined by $\tau_{zx,x}(x_T, z)$. The deeper the center of mass of $\tau_{zx,x}(x_T, z)$, the larger the ΔGPE (for a given deflection).

The red lines in Fig. 4 show the implications of trying to apply the lithostatic approximation for the trench column (i.e. assuming $\tau_{zx,x}(x_T, z) = 0$). In this case there is no equilibration of the vertical normal stress - $\Delta\sigma_{zz}$ does not converge with depth. The red line in right hand panel represents the true ΔGPE. However, in terms of the horizontal force balance, the value of the true ΔGPE is meaningless, as it does not represent the actual state of stress with depth.

5 Discussion

Several previous studies have discussed the existence of a pressure deficit (ΔP_T) due to the downbending of the trailing plane and the potential for a resulting component of net slab pull (Richter et al., 1977; Bird et al., 2008; Bercovici et al., 2015). To the best of the author's knowledge, no prior study has systematically analysed the underlying mechanics or quantitatively estimated the magnitude of the trench pull force. Richter et al. (1977) noted that *it is not even clear whether any of the pressure reduction is available to drive the plates* (see longer quote in the introduction). The answer provided by the current study is that some of that pressure reduction is available. Specifically, it is the center of mass of $\tau_{zx,x}(x_T, z)$, which controls the length scale over which the trench pressure deficit acts. Based on insights from simple mechanical models, the center of mass is suggested to be $\frac{z'_m}{2} \approx z'_{np}$. This yields an trench pull force of ≈ 2.5 TN/m, based on reference parameters given in Table 1.

It is notable that this estimate is similar to the predicted magnitude of the ridge push force. The implication is that the topography associated with zones of divergence and convergence contributes a similar net driving force in the boundary layer (e.g, Hager and O'Connell (1981); Bercovici et al. (2015)). It follows that the total topographic driving force (ΔGPE* between ridge and trench) may be around 5 $\mathrm{TN\,m^{-1}}$. Assuming shear stresses beneath the oceanic lithosphere are 1 MPa, the estimated total ΔGPE* is enough to balance the basal drag force on a plate of about 5000 km, a fairly typical length scale for Earth's subducting plates. There are many studies that infer basal shear stress of significantly less than this, in the range of 0.2-0.5 MPa (Lister, 1975; Melosh, 1977; Richter et al., 1977; Wiens & Stein, 1985; Chen et al., 2021). On the other hand, trench and ridge systems do not sum perfectly constructively on Earth. For the Pacific Plate in the Cenozoic, there is about 50 % constructive contribution to the tangential component of the torque vector, based on trench geometry (Sandiford et al., 2024). For idealised plate geometries, however, the total ΔGPE* is sufficient to balance a resisting basal drag, within the uncertainties associated with the latter.

In developing a model for the depth distribution of the relevant stress quantities (i.e. $\tau_{zx,x}(z)$) various assumptions and simplifications have been made. Following the standard thin plate approach we neglect any dynamic-topography contribution to the trench deflection and assume that the basal boundary is shear stress free. The mechanical models neglect plate rotation due to deflection, and assume uniform constitutive properties. These choices all preserve the symmetry in the resulting stress distributions (e.g., Fig. 3). Some of these assumptions could be removed with a more sophisticated analytic treatment. Comparison with numerical subduction models which solve the same stress equilibrium equation (e.g., Eq. 2), but are not constrained by as many simplifying assumptions, may also be informative.

Sandiford and Craig (2023) analysed the vertically integrated horizontal force balance based on the output of a 2D subduction model. The model was based on the finite element method, the depth of the domain represented the entire mantle, and no plate velocities were imposed. Note that although the current study uses a slightly different symbol convention compared with Sandiford and Craig (2023) the underlying integral definitions are identical in each case (e.g., Eq. 7). The trench pull force calculated from vertical integration of $\sigma_{zz}(z)$, was about 2.0 $\mathrm{TN\,m^{-1}}$ relative to a column of isostatic lithosphere in the trailing plate. Additional information provided in that paper gives the trench depth as $w_T \sim 2.5$ km (relative to the isostatic level) and the neutral plane depth $z'_{np} \sim$ 32 km. Applying Eq. 27 gives $\sim$ 2.6 $\mathrm{TN\,m^{-1}}$. The accuracy of the scaling expression is $\sim$ 75 % as applied to this particular model and timestep. Regarding the two distinct modes via which a net slab pull can be generated (as discussed in Section 1) it is of considerable interest to compare estimates of the trench pull force with the value of F_D evaluated at the trench. In the model presented in Sandiford and Craig (2023) F_D was weakly positive at the trench ($\sim$ 0.6 $\mathrm{TN\,m^{-1}}$), indicating that the net slab pull was trench-pull (rather than tension) dominated. It should be straightforward to test the generality of these ideas by others in the subduction modeling community.

Bessat et al. (2020) estimated the horizontal variation of the *true* GPE based on a set of numerical subduction models. The models were based on the finite-difference method, the domain represented the upper mantle, and various velocity boundary conditions were described in the study. The variation of the GPE around the trench was estimated to be in excess of 50 $\mathrm{TN\,m^{-1}}$. Note that the base of the model was chosen as vertical integration depth (z_c). As highlighted in Fig. 4, for non-isostatic topography the (theoretical) lithostatic pressure is not a suitable proxy for the vertical normal stress. When either of the columns is non-isostatic the difference in integrated lithostatic pressure does not converge, and very large but essentially meaningless values are expected if the integration is continued to arbitrary depths. It is speculated that, had the true vertical normal stress from the numerical model been used, instead of the lithostatic pressure, values compatible with Eq. 27 would have been obtained.

6 Conclusions

The purpose of this paper has been to investigate the mechanics and typical magnitude of the trench pull force. The description of a net horizontal force due to gravitational potential energy differences is extended to non-isostatic columns by introducing a corrected density $\rho^*(z)$ which incorporates the effects of vertical shear stress gradients ($\tau_{zx,x}(z)$) as a pseudo-density $\hat{\rho}(z)$. The integral of the corrected lithostatic pressure $\bar{P}_L^*$ provides the corrected GPE*, which is equal to $-\bar{\sigma}_{zz}$. It is shown that the ΔGPE* depends on the dipole moment of the difference in corrected density $\Delta\rho^*(z)$ between columns, in an analogous way to the isostatic case. For a given trench deflection (w_T), the magnitude of the trench pull force is controlled by the vertical center of mass of the shear stress gradient in the column at the trench. Elastic and elasto-plastic models are used to investigate this problem, specifically the distribution of $\tau_{zx,x}(z)$. These models highlight the tendency for $\tau_{zx,x}(z)$ to concentrate near the center of the strong portion of the plate. Extrapolating to the lithosphere, it is assumed that the center of mass $\tau_{zx,x}(z)$ lies at $\sim \frac{z'_m}{2} \approx z'_{np}$. The resulting estimate is about 2.5 $\mathrm{TN\,m^{-1}}$, similar to that associated with isostatic cooling of old lithosphere. The total topographic driving force between ridges and trenches is likely to be associated with a net force of around 5 $\mathrm{TN\,m^{-1}}$, enough to balance basal drag of 1 MPa, over a plate length of 5000 km.

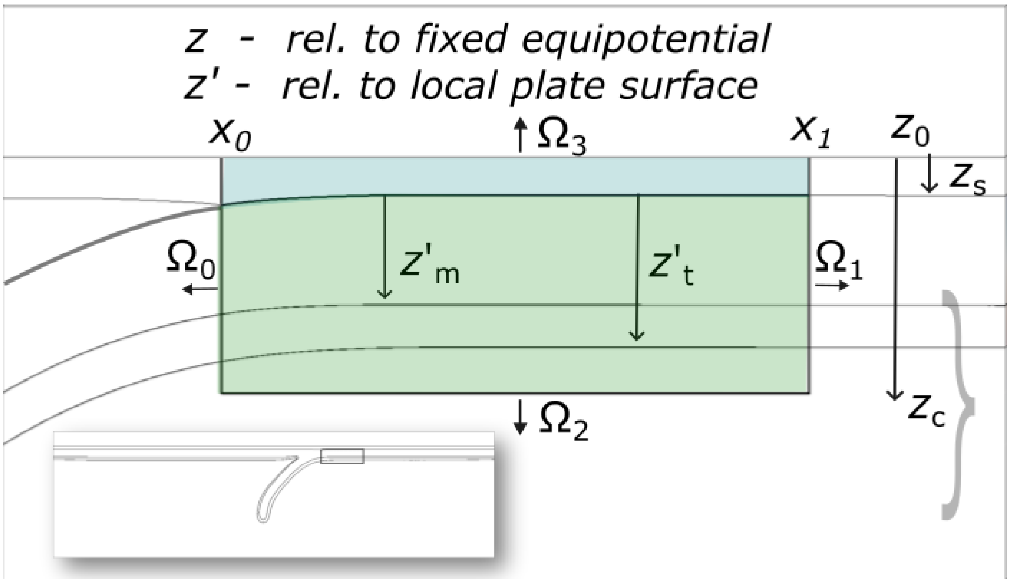

Figure 1. Domain used to develop the vertically integrated horizontal force balance (e.g. Eq. 7). The green region represents rock, the blue region the water column. To simplify the analysis we combine these regions so that Ω_3 is the sea surface (at z_0), but makes no contribution to the horizontal force balance. The vertical boundaries ($\Omega_{0,1}$) extend from z_0 to z_c. z'_m represents the mechanical thickness of the lithosphere, typically significantly less than the thermal thickness z'_t. The level given by z_c represents the integration depth for the vertically-integrated force balance. The assumption is that z_c is sufficiently large that differences in vertical normal stresses can be neglected, i.e. that z_c represents a compensation level. If this condition holds, the respective terms in the vertically integrated force balance will converge with larger z_c. A initial reference value of $z_c \sim z'_t$ 100 km is used, but an important conclusion is that equilibration occurs at significantly shallower depths ($\leqslant z'_m$).

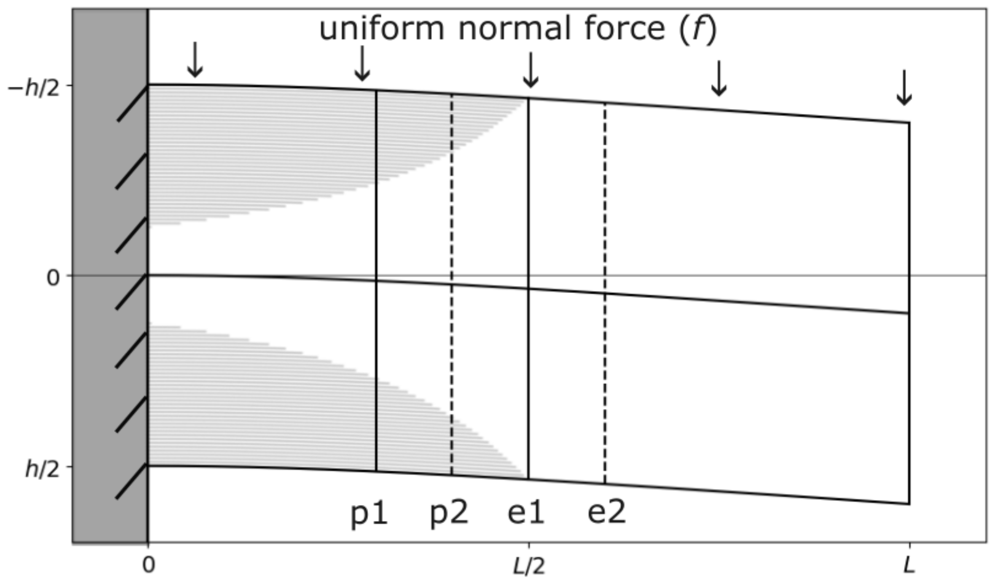

Figure 2. Deflection of a cantilever subject to uniform vertical normal force. The dimensional deflection is: $w(x) = \frac{fx^2}{24EI}\left(6L^2 - 4Lx + x^2\right)$, where f is the normal force. In this figure, f and L are taken as 1, the aspect ratio is 2, and E is chosen to provide a dimensionless deflection $w' = \frac{w}{L}$ of 5%. The general behavior can be represented by scaling stresses by the maximum values: for the horizontal normal stress, $\sigma_{xx}^{Max} = \frac{6fL^2}{h^2}$, and for the shear stresses, $\tau_{xz}^{Max} = \frac{3fL}{2h}$. This is how the stresses along profiles (p1, p2, e1, e2) are represented in Fig. 3. The light grey region shows the zone where yielding is assumed, with the yield limit given by $\tau_{\mathrm{Max}} <= \frac{1}{2}\sigma_{xx}^{Max}$.

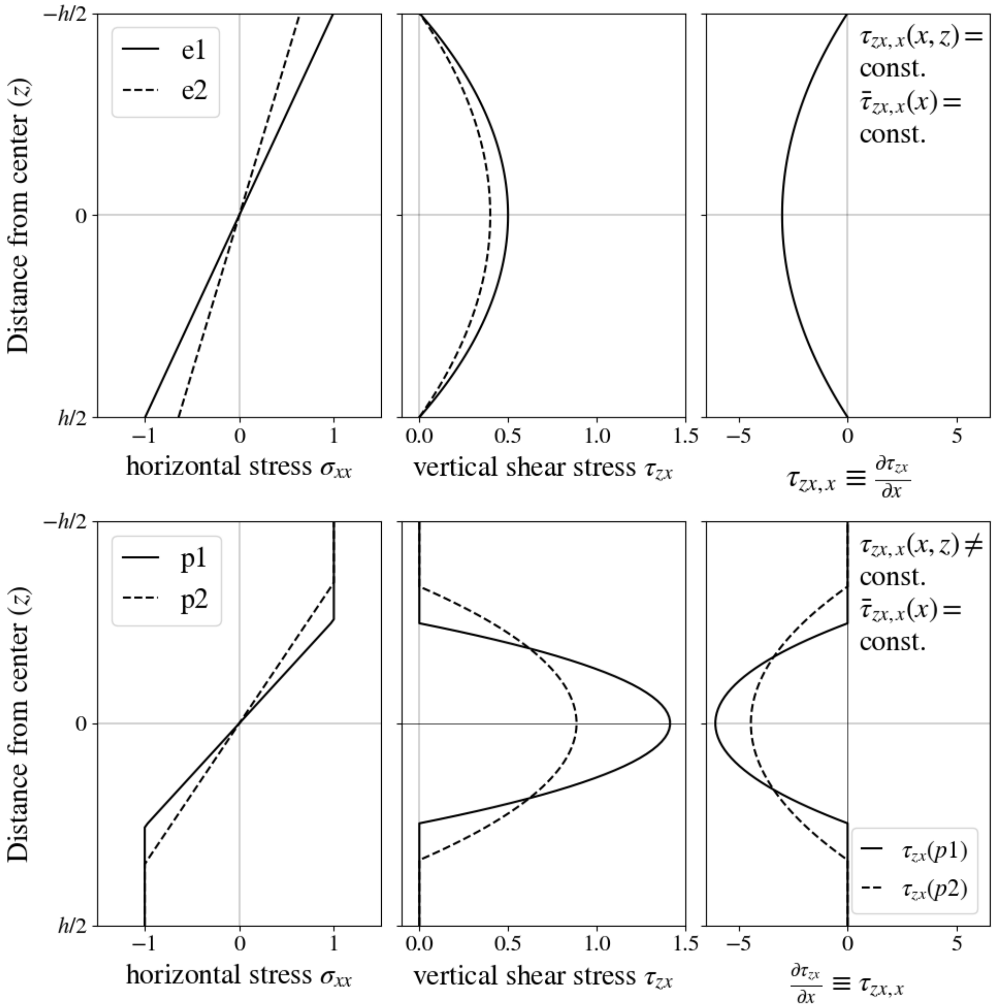

Figure 3. Stress distribution in elastic (upper panels), and elasto-plastic (lower panels) domains, after Horne (1951). Normal stresses are scaled using the prescribed value of the yield stress $\sigma_y = \frac{1}{4}\sigma_{xx}^{Max}$; shear stresses are scaled using $\frac{1}{2}\tau_{zx}^{Max}$, as discussed in the Fig. 2 caption. Of particular importance are the right hand panels, showing the horizontal gradient of the vertical shear stress ($\tau_{zx,x}(z)$). The assumption of uniform loading implies that the vertical shear stress resultant is constant ($\bar{\tau}_{zx,x} \equiv \frac{dV}{dx} = f$). In the elastic domain, $\tau_{zx,x}(x,z)$ is constant everywhere, as shown in the top right hand panel. In the yielding case, $\tau_{zx,x}(x,z)$ varies as the elastic core narrows, however the resultant ($\bar{\tau}_{zx,x}$) remains constant.

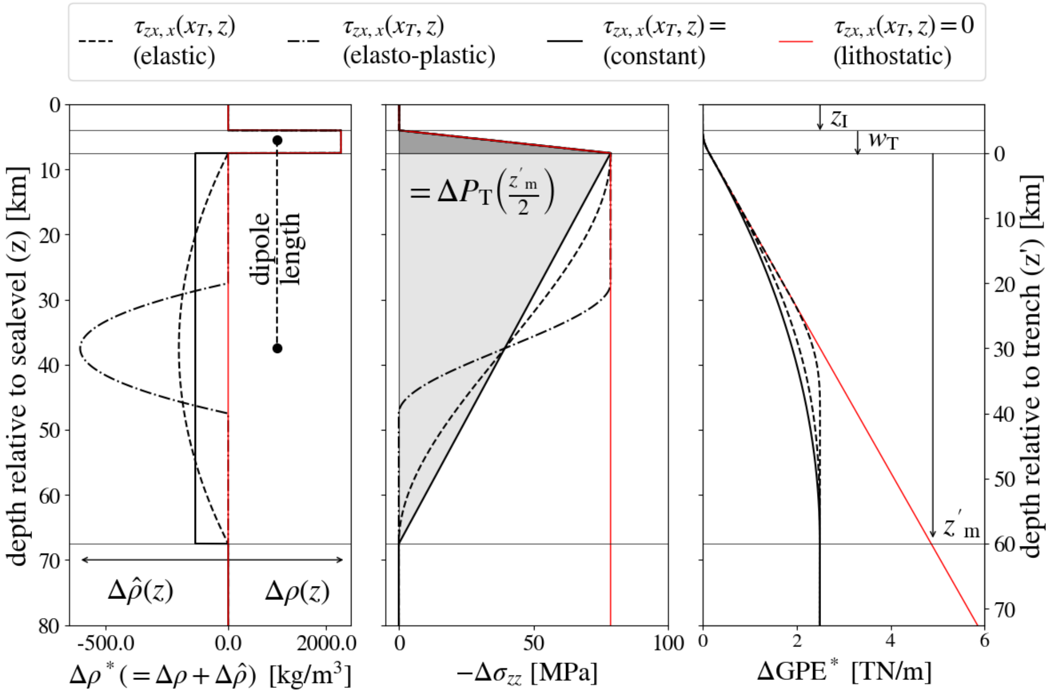

Figure 4. Each panel represents a difference in quantities between the isostatic reference column and a column beneath the trench. The left hand panel shows $\Delta\rho^*(z)$: the difference in the corrected density between the columns. This is the sum of, respectively, the difference in the true density ($\Delta\rho(z)$) and the pseudo density ($\Delta\hat{\rho}(z)$). Horizontal scales are unequal. The assumption of $\tau_{zx,x}(x_I, z) = 0$ means $\Delta\hat{\rho}(z) = -\hat{\rho}(x_T, z)$ with $\hat{\rho}(x_T, z) \propto \tau_{zx,x}(x_T, z)$). Hence, $\Delta\rho^*(z)$ is completely specified by the assumed distribution of $\tau_{zx,x}(x_T, z)$. 4 different models for $\tau_{zx,x}(x_T, z)$ are plotted as indicated in the legend. The dipole moment of $\Delta\rho^*(z)$ gives the ΔGPE* (from Eq. 19). The dipole depth extent is shown schematically, and is controlled by the vertical center of mass of $\tau_{zx,x}(x_T, z)$. The middle panel shows the (negative of) the difference in vertical normal stress. The trench pull force represents the area bounded by $-\Delta\sigma_{zz}(z)$ ($\equiv\Delta$GPE*); all models shown with black lines bound identical area. The mathematical expression represents the area of the light gray triangle, (the approximate value of the trench pull force, neglecting the dark triangle, e.g., Eq. 27). The hydrostatic assumption implies that differences in $\Delta\sigma_{zz}$ equilibrate exactly. When the lithostatic approximation is used for the trench column (shown in red) the vertical normal stress does not equilibrate. The right hand panel shows the cumulative ΔGPE$^*(z)$. In the lithostatic approximation, the ΔGPE* is unbounded. The figure uses reference values shown in Table 1.

Appendix A Distribution of vertical shear stress

In deriving the vertical distribution of the shear stress, the assumptions are a uniform 2D plate of thickness h, which undergoes plane bending, with zero shear stress on the top and bottom edges. We retain the same coordinate convention (positive down, to the right); Here, the origin of z is the center of the plate. Neglecting any in-plane stress resultant, the balance of moments and vertical forces, for a 2D beam/plate equation are expressed as:

$$\frac{dM}{dx} = V(x), \; \frac{dV}{dx} = -f(x) \tag{A1}$$

The normal stress $\sigma_{xx}(z)$ due to bending is:

$$\sigma_{xx}(x,z) = -\frac{M(x) \cdot z'}{I} \tag{A2}$$

where I is the second moment of area (per unit length):

$$I = \int_{-\frac{h}{2}}^{\frac{h}{2}} z^2 \, dz \tag{A3}$$

Combining Eq. A1 & A2, the horizontal gradient of normal stress can be written:

$$\frac{\partial \sigma_{xx}(x,z)}{\partial x} = -\frac{z \cdot V(x)}{I} \tag{A4}$$

the stress equilibrium equation is:

$$\frac{\partial \sigma_{xx}}{\partial x} + \frac{\partial \sigma_{xz}}{\partial z} = 0 \tag{A5}$$

so that:

$$\frac{\partial \tau_{xz}}{\partial z} = \frac{z \cdot V(x)}{I} \tag{A6}$$

Integrating with respect to z yeilds:

$$\tau_{xz}(x,z) = \int \frac{z \cdot V(x)}{I} \, dz = \frac{V(x)}{I} \left(\frac{z^2}{2} \right) + C(x) \tag{A7}$$

Given $\tau_{xz}(x, \pm\frac{h}{2}) = 0$, we can solve for $C(x)$:

$$\tau_{xz}(x,z) = \frac{V(x)}{I} \left(\frac{z^2}{2} - \frac{h^2}{8} \right) \tag{A8}$$

Symmetry of the stress tensor means that the vertical shear stress τ_{zx} follows the same distribution as τ_{xz}. The maximum value of the vertical shear stress occurs at the center of the plate (or more generally, at the neutral plane), where the horizontal stress is zero. Across the plate, the principal stresses rotate: they are only truly vertically aligned (Andersonian) at the free surface. At the center of the plate, the principal stresses are oriented at 45° from the horizontal: the differential stress is not zero at the middle of the plate, although the quantity σ_{xx} is. In the case of the lithosphere, where σ_{xx} includes a large lithostatic means stress, it is the stress difference that goes to zero across the neutral plane: $(\sigma_{xx} - \sigma_{zz}) = (\tau_{xx} - \tau_{zz}) = 0$.

Appendix B ΔGPE* as the dipole moment of $\Delta\rho^*$

In the manuscript, the ΔGPE* between an isostatic reference column, and a deflected column, is given by:

$$\Delta\text{GPE}^* = g\int_{z_0}^{z_c} \Delta\rho^*(z)(z_c - z)dz \tag{B1}$$

the hydrostatic approximation requires that the mass (first moment) of the true(ρ) and pseudo ($\hat{\rho}$) contributions to $\Delta\rho^*(z)$ are equal:

$$M = \int_{z_0}^{z_c} \Delta\rho(z)\,dz = -\int_{z_0}^{z_c} \Delta\hat{\rho}(z)dz = (\rho_m - \rho_w)w(x) \tag{B2}$$

where $w(x)$ is the deflection. The difference in the center of mass of each of these distributions (around z_c) can be written as:

$$\begin{aligned}\Delta z_{\text{cm}} = &\frac{1}{M}\int_{z_0}^{z_c} \left(\Delta\rho(z)(z_c - z)\right)dz \\ - \\ &-\frac{1}{M}\int_{z_0}^{z_c} \left(\Delta\hat{\rho}(z)\right)(z_c - z)dz\end{aligned} \tag{B3}$$

the negative sign on the last line reflects the fact that $\Delta\rho^*(z)$ is a negative quantity, and we wish to define a positive center of mass. Which means we can write Eq. B1 as:

$$\Delta\text{GPE}^* = gM\Delta z_{\text{cm}} \tag{B4}$$

$$\Delta\text{GPE}^* = (\rho_m - \rho_w)gw(x)\Delta z_{\text{cm}} \tag{B5}$$

$$\tag{B6}$$

The center of mass of $\Delta\rho(z)$ is given by $z_I - \frac{1}{2}w_T$. Based on the models and assumptions developed in this paper, the center of mass of $\hat{\rho}(z)$ (being identical to that of $\tau_{zx,x}(z)$) occurs at $z_I + w + \frac{1}{2}z'_m$. The difference is $\frac{1}{2}(w + z'_m)$, as in Eq. 27. Eq. B1 and B6 are statements that the ΔGPE* is equal to dipole moment of the difference in corrected density ($\Delta\rho^*$) between two columns.

This relationship also allows us to examine the approximation we used in neglecting the crust. Because we neglected the crust, and instead treated the entire column of lithosphere as having background mantle density, we introduced an error in the distribution of $\Delta\rho$. We overestimated the $\Delta\rho$ in the section of lithosphere between z_I and w_T, because we took the density difference as $\rho_m - \rho_m$, whereas the actual density difference is $\rho_m - \rho_c$ (assuming the moho depth is greater than w_T, which is usually correct). This overestimate is balanced by an equal underestimate between the depths $z_I + z'_m$ and $z_I + z'_m + w_T$, where the isostatic column contains mantle rock and the deflected column contains crust. The error in the GPE* can be estimated from Eq. B6, and is $\approx$ 0.04 $\text{TN}\,\text{m}^{-1}$.

Open Research Section

This manuscript does not contain any new data.

Acknowledgments

This work would not have been possible without support of my partner. I would also like to acknowledge the support of Pete Betts, Sara Polanco, Rebecca Farrington and Mark Quigley.

References

Bercovici, D., Tackley, P., & Ricard, Y. (2015). 7.07-the generation of plate tectonics from mantle dynamics. *Treatise on Geophysics. Elsevier, Oxford*, 271–318.

Bessat, A., Duretz, T., Hetényi, G., Pilet, S., & Schmalholz, S. M. (2020). Stress and deformation mechanisms at a subduction zone: insights from 2-d thermo-mechanical numerical modelling. *Geophysical Journal International*, *221*(3), 1605–1625.

Bird, P. (1998). Testing hypotheses on plate-driving mechanisms with global lithosphere models including topography, thermal structure, and faults. *Journal of Geophysical Research: Solid Earth*, *103*(B5), 10115–10129.

Bird, P., Liu, Z., & Rucker, W. K. (2008). Stresses that drive the plates from below: Definitions, computational path, model optimization, and error analysis. *Journal of Geophysical Research: Solid Earth*, *113*(B11).

Caldwell, J., Haxby, W., Karig, D. E., & Turcotte, D. (1976). On the applicability of a universal elastic trench profile. *Earth and Planetary Science Letters*, *31*(2), 239–246.

Chapple, W. M., & Forsyth, D. W. (1979). Earthquakes and bending of plates at trenches. *Journal of Geophysical Research: Solid Earth*, *84*(B12), 6729–6749.

Chen, Y.-W., Colli, L., Bird, D. E., Wu, J., & Zhu, H. (2021). Caribbean plate tilted and actively dragged eastwards by low-viscosity asthenospheric flow. *Nature Communications*, *12*(1), 1603.

Coblentz, D., van Wijk, J., Richardson, R. M., Sandiford, M., Foulger, G., Lustrino, M., & King, S. (2015). The upper mantle geoid: Implications for continental structure and the intraplate stress field. *Geological Society of America Special Papers*, *514*, 197–214.

Davies, G. F. (2022). Stories from the deep earth.

Drucker, D. (1956). The effect of shear on the plastic bending of beams.

Fleitout, L., & Froidevaux, C. (1983). Tectonic stresses in the lithosphere. *Tectonics*, *2*(3), 315–324.

Garcia, E. S. M., Sandwell, D. T., & Bassett, D. (2019). Outer trench slope flexure and faulting at pacific basin subduction zones. *Geophysical Journal International*, *218*(1), 708–728.

Goodier, J. N., & Timoshenko, S. (1970). *Theory of elasticity*. McGraw-Hill.

Grellet, C., & Dubois, J. (1982). The depth of trenches as a function of the subduction rate and age of the lithosphere. *Tectonophysics*, *82*(1-2), 45–56.

Hager, B. H., & O'Connell, R. J. (1981). A simple global model of plate dynamics and mantle convection. *Journal of Geophysical Research: Solid Earth*, *86*(B6), 4843–4867.

Horne, M. R. (1951). The plastic theory of bending of mild steel beams with particular reference to the effect of shear forces. *Proceedings of the Royal Society of London. Series A. Mathematical and Physical Sciences*, *207*(1089), 216–228.

Lemenkova, P. (2019). Geomorphological modelling and mapping of the peru-chile trench by gmt. *Polish Cartographical Review*, *51*(4), 181–194.

Lister, C. R. (1975). Gravitational drive on oceanic plates caused by thermal contraction. *Nature*, *257*(5528), 663–665.

McNutt, M. K., & Menard, H. (1982). Constraints on yield strength in the oceanic lithosphere derived from observations of flexure. *Geophysical Journal International*, *71*(2), 363–394.

Melosh, J. (1977). Shear stress on the base of a lithospheric plate. *Stress in the Earth*, 429–439.
Molnar, P., & Lyon-Caen, H. (1988). Some simple physical aspects of the support, structure, and evolution of mountain belts.
Parsons, B., & Molnar, P. (1976). The origin of outer topographic rises associated with trenches. *Geophysical Journal International*, *45*(3), 707–712.
Richter, F., McKenzie, D., et al. (1977). Simple plate models of mantle convection. *Journal of Geophysics*, *44*(1), 441–471.
Sandiford, D., Betts, P., Whittaker, J., & Moresi, L. (2024). A push in the right direction: Exploring the role of zealandia collision in eocene pacific-australia plate motion changes. *Tectonics*, *43*(3), e2023TC007958.
Sandiford, D., & Craig, T. J. (2023). Plate bending earthquakes and the strength distribution of the lithosphere. *Geophysical Journal International*, *235*(1), 488–508.
Schmalholz, S. M., Medvedev, S., Lechmann, S. M., & Podladchikov, Y. (2014). Relationship between tectonic overpressure, deviatoric stress, driving force, isostasy and gravitational potential energy. *Geophysical Journal International*, *197*(2), 680–696.
Tanimoto, B. (1957). Stress analysis of a gravitating simply-supported beam. , *7*, 15–20.
Turcotte, D. L., McAdoo, D., & Caldwell, J. (1978). An elastic-perfectly plastic analysis of the bending of the lithosphere at a trench. *Tectonophysics*, *47*(3-4), 193–205.
Turcotte, D. L., & Schubert, G. (2002). *Geodynamics*. Cambridge university press.
Watts, A. B. (2001). *Isostasy and flexure of the lithosphere*. Cambridge University Press.
Wiens, D. A., & Stein, S. (1985). Implications of oceanic intraplate seismicity for plate stresses, driving forces and rheology. *Tectonophysics*, *116*(1-2), 143–162.
Zhang, F., Lin, J., & Zhan, W. (2014). Variations in oceanic plate bending along the mariana trench. *Earth and Planetary Science Letters*, *401*, 206–214.